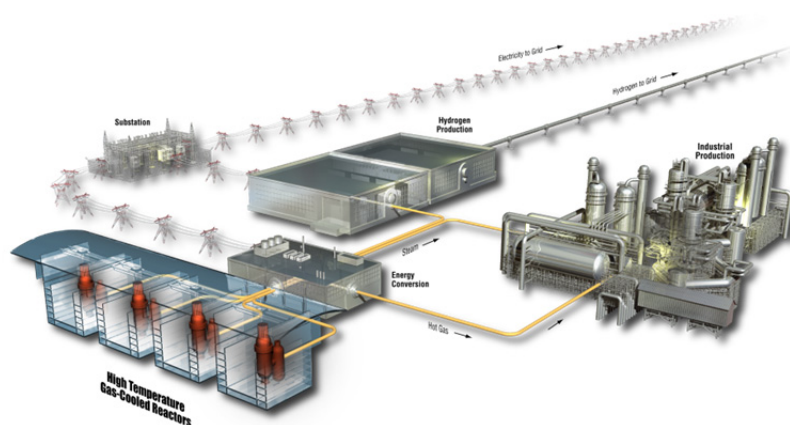


# Progress Report on Long Hold-Time Creep-Fatigue of Alloy 617 at 850°C

L. Carroll

October 2015

The INL is a  
U.S. Department of Energy  
National Laboratory  
operated by  
Battelle Energy Alliance



#### **DISCLAIMER**

This information was prepared as an account of work sponsored by an agency of the U.S. Government. Neither the U.S. Government nor any agency thereof, nor any of their employees, makes any warranty, expressed or implied, or assumes any legal liability or responsibility for the accuracy, completeness, or usefulness, of any information, apparatus, product, or process disclosed, or represents that its use would not infringe privately owned rights. References herein to any specific commercial product, process, or service by trade name, trade mark, manufacturer, or otherwise, does not necessarily constitute or imply its endorsement, recommendation, or favoring by the U.S. Government or any agency thereof. The views and opinions of authors expressed herein do not necessarily state or reflect those of the U.S. Government or any agency thereof.

# **Progress Report on Long Hold-Time Creep-Fatigue of Alloy 617 at 850°C**

**L. Carroll**

**October 2015**

**Idaho National Laboratory  
INL ART TDO Program  
Idaho Falls, Idaho 83415**

**<http://www.inl.gov>**

**Prepared for the  
U.S. Department of Energy  
Office of Nuclear Energy  
Under DOE Idaho Operations Office  
Contract DE-AC07-05ID14517**



## INL ART TDO Program

# Progress Report on Long Hold-Time Creep-Fatigue of Alloy 617 at 850°C

INL/EXT-15-35132

October 2015

Author:



Laura J. Carroll  
INL ART TDO Senior Staff Scientist

10-6-15

Date

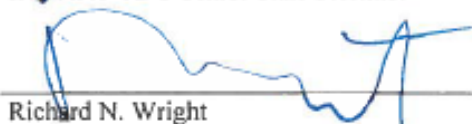
Approved by:



Jill K. Wright  
INL ART TDO Senior Staff Scientist

10-6-15

Date



Richard N. Wright  
INL ART TDO High Temperature Materials Lead

10/6/2015

Date



Travis R. Mitchell  
INL ART TDO Relationship Manager

10/6/2015

Date



Alan L. Trost  
INL ART TDO Quality Assurance Lead

10/13/2015

Date



## **ABSTRACT**

Alloy 617 is the leading candidate material for an intermediate heat exchanger for the very high temperature reactor. To evaluate the behavior of this material in the expected service conditions, strain-controlled cyclic tests that include long hold times up to 240 minutes at maximum tensile strain were conducted at 850°C. In terms of the total number of cycles to failure, the fatigue resistance decreased when a hold time was added at peak tensile strain. Increases in the tensile hold duration degraded the creep-fatigue resistance, at least to the investigated strain controlled hold time of up to 60 minutes at the 0.3% strain range and 240 minutes at the 1.0% strain range. The creep-fatigue deformation mode is considered relative to the lack of saturation, or continually decreasing number of cycles to failure with increasing hold times. Additionally, preliminary values from the 850°C creep-fatigue data are calculated for the creep-fatigue damage diagram and have higher values of creep damage than those from tests at 950°C.





## **ACKNOWLEDGEMENTS**

The author would like to thank Sam Sham, Mark Carroll, Jill Wright, and Richard Wright for thoughtful guidance and discussions regarding this subject matter. The author would also like to acknowledge Joel Simpson and Randy Lloyd for conducting the extensive creep-fatigue testing, Tammy Trowbridge and Todd Morris for the considerable metallurgical work required for this study, and Jill Wright and Nancy Lybeck for data analysis of the fatigue and creep-fatigue cyclic testing. The author would like to thank Mark Carroll for the transmission electron microscopy analysis. The transmission electron microscopy work was carried out at the Boise State Center for Materials Characterization, supported by NSF MRI Grant DMR-0521315, and at the Center for Advanced Energy Studies Microscopy Analysis and Characterization Suite. This work was supported through the U.S. Department of Energy Office of Nuclear Energy.



# CONTENTS

ABSTRACT.....	vii
ACKNOWLEDGEMENTS.....	ix
ACRONYMS.....	xiii
1. INTRODUCTION.....	1
2. EXPERIMENTAL PROCEDURE.....	3
3. RESULTS.....	4
3.1 Macroscopic Deformation Behavior.....	4
3.2 Deformed Microstructures.....	7
3.3 Dislocation Substructures.....	9
4. DISCUSSION.....	11
4.1 Creep-Fatigue Saturation.....	11
4.2 Cyclic Softening.....	14
4.3 Damage Diagram.....	14
5. CONCLUSIONS.....	17
6. REFERENCES.....	18

# FIGURES

Figure 1. The number of cycles to failure as a function of hold time in fatigue and creep-fatigue of Alloy 617 at 950°C at 0.3%, 0.6 %, and 1.0% total strain. ....	2
Figure 2. Schematics of the strain versus time waveforms for fatigue (a) and tensile-hold creep-fatigue (b). ....	3
Figure 3. The number of cycles to failure as a function of hold time in fatigue and creep-fatigue of Alloy 617 at 850°C at 0.3% and 1.0% total strain. ....	4
Figure 4. A midlife fatigue and 30-minute hold creep-fatigue hysteresis loops from selected tests at 850°C and 0.3% total strain (a). A midlife stress relaxation fit for the peak tensile strain controlled hold time at 850°C and 0.3% total strain (b). ....	5
Figure 5. Stress versus hold time during the strain controlled hold for a midlife cycle of a 1.0% total strain creep-fatigue test with a 240-minute hold time. ....	5
Figure 6. Peak tensile and compressive stresses as a function of cycle for selected continuous-cycle fatigue and creep-fatigue tests at 850 °C and 0.3% (a) and 1.0% (b) total strain. ....	6
Figure 7. A transgranular surface crack in a 0.3% total strain fatigue specimen cycled at 850°C (a). An intergranular surface crack in a 0.3% total strain, 30-minute hold creep-fatigue	

specimen cycled at 850°C (b). The specimen surface is not shown in (b) but is to the left of the image.....	8
Figure 8. Acicular carbides on an internal grain boundary (a) and grain boundary cavitation/cracking (b) in a creep-fatigue specimen tested at 0.3% total strain and a 3-minute hold time at 850°C.....	8
Figure 9. A plot of the peak stress versus cycle data with the progression of the interior grain boundary cracking superimposed from a creep-fatigue specimen tested at 0.3% total strain and a 3-minute hold time at 850°C. ....	9
Figure 10. TEM images from the deformed gage section of creep-fatigue specimens tested at 850°C and the 0.3% total strain range and a 30-minute (a) and a 10-minute (b) peak tensile hold.....	10
Figure 11. TEM images illustrating the subgrain structure in the gage section of continuous-cycle fatigue specimens tested at 850°C and the 0.3% total strain range. ....	10
Figure 12. TEM images from the gage section of creep-fatigue specimens tested at 850°C and the 0.3% total strain range and a 3-minute peak tensile hold at 1,000 cycles (a and b) and 2,000 cycles (c and d) . ....	11
Figure 13. Alloy 617 fatigue and creep-fatigue data from the current work (ART), Rao et al., <sup>4</sup> and Totemeier and Tian <sup>11</sup> (the values of which have been estimated from published papers). The data from Rao <sup>4</sup> was generated in a simulated helium environment and that of Totemeier et al. <sup>11</sup> at 800 and 1000 °C. The 150 minute hold time ART data point at 950 °C and the 0.6% strain range was a runout. ....	13
Figure 14. Preliminary values for the creep-fatigue damage diagram data points calculated for the 850 and 950°C using the midlife cycle to assess the creep damage term and the creep-fatigue envelope (blue line) recommended during the Draft Alloy 617 Code Case. <sup>14</sup> .....	16
Figure 15. Preliminary values for the creep-fatigue damage diagram data points calculated for 850 and 950°C and the creep-fatigue envelope (blue line) recommended during the Draft Alloy 617 Code Case. <sup>14</sup> The 850°C long hold (0.3% strain range and a 30-minute hold time or longer and 1.0% strain range and a 120-minute hold time or longer) data points are a separate data series labeled 850°C – long hold. ....	16
Figure 16. Preliminary values for the creep-fatigue damage diagram data points calculated for the 850 and 950°C and the creep-fatigue envelope (blue line) recommended during the Draft Alloy 617 Code Case. <sup>14</sup> The 0.3% strain range and 3- and 10-minute hold times exhibit the highest D <sub>c</sub> values.....	17

## TABLES

Table 1. The composition in wt% of Alloy 617.....	3
Table 2. Cracking modes observed in fatigue and creep-fatigue specimens tested at 850°C selected for metallurgical evaluation. ....	7

## ACRONYMS

ASME	American Society of Mechanical Engineers
IHX	intermediate heat exchanger
INL	Idaho National Laboratory
PLN	plan
TEM	transmission electron microscopy



# Progress Report on Long Hold-Time Creep-Fatigue of Alloy 617 at 850°C

## 1. INTRODUCTION

Creep-fatigue deformation is expected to be a significant contributor to the potential factors that limit the useful life of the intermediate heat exchanger (IHX) in a very high temperature reactor nuclear system.<sup>1</sup> The IHX of a high-temperature gas reactor will be subjected to a number of transient cycles due to startup and shutdown operations imparting high local stresses on the component. This cycling introduces a creep-fatigue type of interaction as dwell times occur intermittently.

The leading candidate alloy for the IHX is a nickel-base solid solution strengthened alloy, Alloy 617, which must safely operate near the expected reactor outlet temperature of up to 950°C.<sup>1</sup> This solid solution strengthened, nickel-base alloy provides an interesting creep-fatigue deformation case study because it has characteristics of two different alloy systems for which the cyclic behavior has been extensively investigated. Compositionally, it resembles nickel-base superalloys, such as IN100 and IN718, with the exception of its lower levels of aluminum. However, at temperatures above 800°C, the microstructure of Alloy 617 does not contain the ordered  $\gamma'$  or  $\gamma''$  phases. Thus, microstructurally, it is more similar to an austenitic stainless steel, such as 316 or 304, or Alloy 800H comprised of a predominantly solid solution strengthened matrix phase with a dispersion of inter- and intragranular carbides.

Previous studies of the creep-fatigue behavior of Alloy 617 at 950°C indicate that the fatigue life is reduced when a constant strain dwell is added at peak tensile strain.<sup>2,3,4,5</sup> This results from the combination of faster crack initiation occurring at surface-connected grain boundaries due to oxidation from the air environment along with faster crack propagation resulting from the linking of extensive interior grain boundary cracking.<sup>3</sup> Saturation, defined as the point at which further increases in the strain-controlled hold time duration no longer decreases the cycle life, has been observed for Alloy 617 at 950°C at least to the investigated hold times,<sup>2,3</sup> as illustrated through a plot of cycles to failure versus hold time in Figure 1. The 1000°C creep-fatigue data set generated by Totemeier<sup>5</sup> at the 0.3% and 1.0% strain range is consistent in magnitude in terms of the cycles to failure data observed by Carroll et al.,<sup>2,3</sup> as well as the presence of saturation at relatively short hold times. The data from Carroll et al.<sup>2,3</sup> in Figure 1 and Totemeier and Tian<sup>5</sup> are also consistent in magnitude with the data of Rao et al.<sup>4</sup> investigated at the 0.6% strain range. However, it should be noted that saturation in the number of cycles to failure is not observed in the data published by Rao et al.<sup>4</sup> for tensile hold times of up to 120 minutes. The latter testing was in simulated primary-circuit helium gas as opposed to air and a single data point is reported for the longer hold time conditions.

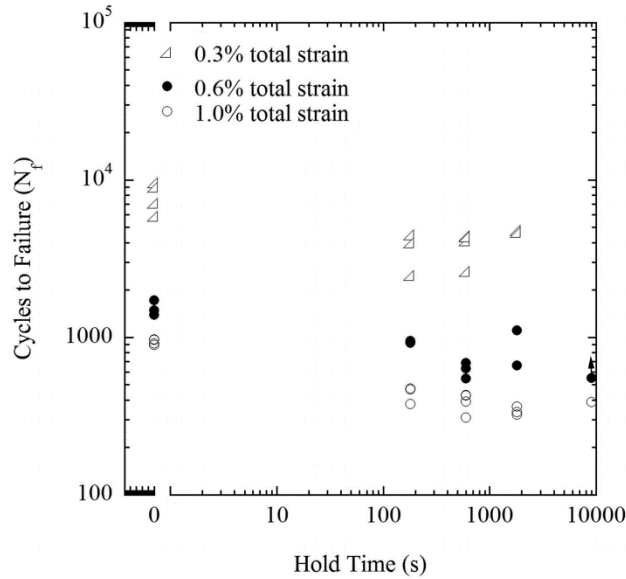


Figure 1. The number of cycles to failure as a function of hold time in fatigue and creep-fatigue of Alloy 617 at 950°C at 0.3%, 0.6 %, and 1.0% total strain.

To further investigate the presence or absence of saturation at 950°C, the deformation mechanisms were considered in detail. The initiation and propagation of a creep-fatigue crack is driven by the combined aspects of creep, fatigue, and environment at the macro-scale. Concurrently, cyclic softening occurs and has been attributed to the formation of subgrains and interior grain boundary cracking.<sup>3</sup> The synergistic influence of the propagating crack and the microstructural evolution ultimately controls the creep-fatigue behavior, thus variations in these deformation modes at the different strain ranges result in different macroscopic properties. For example, in creep-fatigue deformation of Alloy 617 at 950°C and the 0.3% total strain range, the large amount of cracked interior grain boundary interfaces throughout the microstructure in combination with the relatively slow propagation of the grain boundary surface cracks indicates a large influence of creep processes introduced during the strain-controlled tensile hold.<sup>2</sup> Similar to stainless steels,<sup>6,7,8</sup> distinct dislocation subgrain structures develop during creep-fatigue deformation of Alloy 617, initially by the tangling of dislocations into walls. Further cycling allows for dislocation climb, reorganization, and the integration of dislocations from the subgrain interiors along with the evolution into well-ordered hexagonal dislocation networks that form the subboundaries.<sup>3</sup> Both the interior grain boundary cracks and the dislocation substructure rearrangement lead to a pronounced reduction in the peak tensile stress during cycling. Based on the described mechanisms and the rapid stress relaxation to very low magnitudes during the strain controlled hold, it is most likely that creep/plasticity dominates the time-dependent deformation response at 950°C and oxidation due to the air environment plays a relatively minor role, consistent with the apparent saturation in cycles to failure.

The creep-fatigue resistance and deformation mode often vary with temperature. To further assess this, the creep-fatigue behavior of Alloy 617, including the presence or absence of saturation of the number of cycles to failure, was also investigated at 850°C. The progression of creep-fatigue deformation, including the role of the environment and creep damage, was analyzed by examining the stress relaxation response, crack propagation, and dislocation substructures.



## 2. EXPERIMENTAL PROCEDURE

Cylindrical cyclic test specimens, 7.5-mm-diameter in the reduced section with a gage length of 12 mm, were machined from an Alloy 617 annealed plate with the long axis of the specimens aligned along the rolling direction. The composition of the heat of Alloy 617 investigated is given in Table 1. Although the average grain size of the plate is quantified as approximately 150  $\mu\text{m}$ , a significant grain size inhomogeneity is present in the microstructure. All cyclic testing was performed under Idaho National Laboratory (INL) plan PLN-2804.<sup>1</sup>

Table 1. The composition in wt% of Alloy 617.

Ni	C	Cr	Co	Mo	Fe	Al	Ti	Si	Cu	Mn
Bal.	0.05	22.2	11.6	8.6	1.6	1.1	0.4	0.1	0.04	0.1

Fully reversed, strain-controlled continuous-cycle fatigue and tensile-hold creep-fatigue testing was conducted on Alloy 617 at 850°C in air at 0.3% and 1.0% total strain. Continuous-cycle fatigue testing followed a triangular waveform with a strain rate of  $10^{-3}/\text{s}$ . The creep-fatigue testing employed a tensile-hold waveform with a constant strain-controlled hold time at peak tensile strain. Schematics of the fatigue and tensile-hold creep-fatigue waveform are shown in Figure 2. Cyclic tests were conducted in accordance with PLN-3346.<sup>9</sup>

The hold time duration in creep-fatigue varied from as short as 3 minutes to as long as 240 minutes. The number of cycles to failure,  $N_f$ , is defined by the cycle values at which there has been a 20% decrease in the ratio of the peak tensile stress to the peak compressive stress from the point at which this ratio initially deviates from a constant trend. Actual test completion was prior to actual specimen separation, based upon a predetermined drop in load; when the set load drop was detected, the test automatically switched to zero load and power to the heat source was shut off. The microstructural development at the 0.3% strain range and a 3-minute tensile-hold creep-fatigue condition was studied through testing of multiple specimens with specific interruptions, whereby the test was stopped and the specimen removed for direct evaluation of microstructural evolution at representative intermediate points during cyclic deformation. The creep-fatigue tests were interrupted at 1,000, 1,500 and 2,000 cycles.

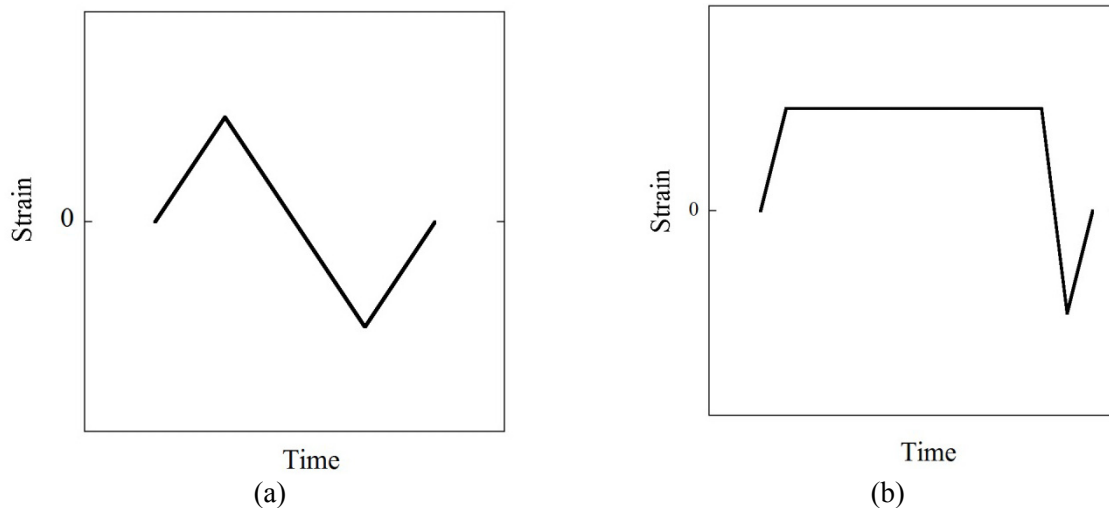


Figure 2. Schematics of the strain versus time waveforms for fatigue (a) and tensile-hold creep-fatigue (b).

The gage sections of the deformed specimens were cut into two halves along the stress axis to expose a plane containing the largest observed surface crack. Half of the gage section was mounted, polished, and etched with a 2% bromine and 98% methanol solution. Metallurgical evaluation was conducted using optical microscopy and a Quanta 650 field emission gun scanning electron microscope. The remaining half of the gage section was mechanically thinned for the extraction of transmission electron microscopy (TEM) foils. The longitudinal portion of the gage section was first reduced to approximately 125  $\mu\text{m}$  and then punched into 3-mm discs. The discs were electropolished using a twin jet TenuPol-5 polisher with a solution of 10% perchloric acid in ethanol at approximately -15°C. Microstructural characterization was conducted using a JEOL JEM-2010 HR analytical TEM operating at 200 kV and a Tecnai TF30-FEG STwin scanning TEM.

### 3. RESULTS

#### 3.1 Macroscopic Deformation Behavior

Fatigue and creep-fatigue tests of Alloy 617 at 850°C at the 0.3 and 1.0% total strain range were conducted in air. Constant strain hold times as long as 60 and 240 minutes, respectively, were introduced at peak tensile strain in creep-fatigue. The cycles to failure are illustrated as a function of hold time in Figure 3. The addition of a strain-controlled tensile hold decreases the total number of cycles to failure relative to continuous-cycle fatigue. A dramatic degradation in cycle life, a factor of 5, occurs at the 0.3% total strain range with a 3-minute hold time. This is much more substantial than the degradation in life between the fatigue and 3-minute hold condition at the 1.0% strain range. At the 1.0% strain range, the number of cycles to failure progressively decreases with longer hold times. A 30-minute hold time drops the number of cycles to failure in half at the 1.0% strain range. Saturation, defined as the point at which further increases in the strain-controlled hold time duration no longer decreases the cycle life, is not observed for either the 0.3 or 1.0% strain ranges for the investigated hold durations.

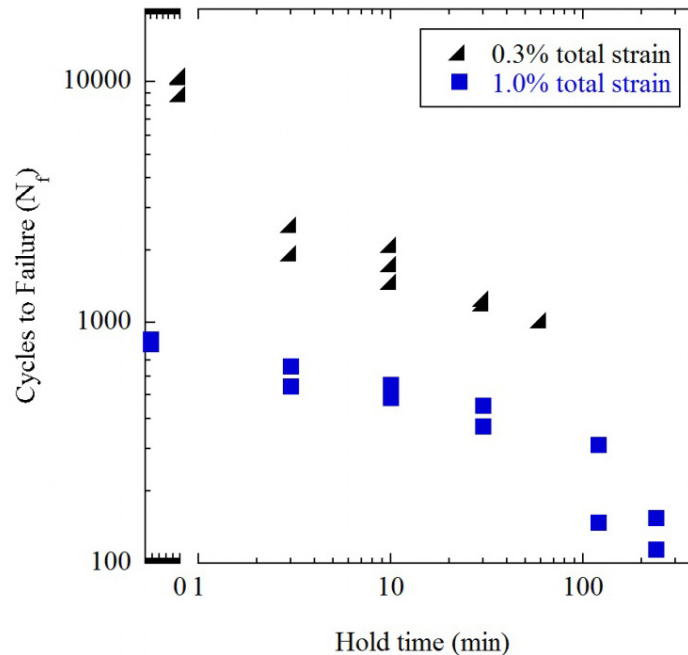


Figure 3. The number of cycles to failure as a function of hold time in fatigue and creep-fatigue of Alloy 617 at 850°C at 0.3% and 1.0% total strain.

The dramatic difference in the number of cycles to failure between fatigue and creep-fatigue at the 0.3% strain range is consistent with the characteristically different hysteresis loops. In fatigue, the stress-strain loop is narrow with limited plasticity; however, the 30-minute-loop is approximately three times wider exhibiting substantially more inelastic strain, as shown in Figure 4(a). The inelastic strain range increases with increasing hold time consistent with the fact that the stresses do not fully relax during the strain-controlled hold, as shown in the schematic of the midlife cycle stress relaxation behavior of a selected 0.3% strain range test in Figure 4(b). The relaxed stress (stress at the end of the hold time) approaches zero with increasing hold durations. Similarly rapid stress relaxation is observed at the 1.0% total strain range, shown for the 240-minute hold time condition in Figure 5; however, the stresses do plateau by hold times of approximately 120 minutes.

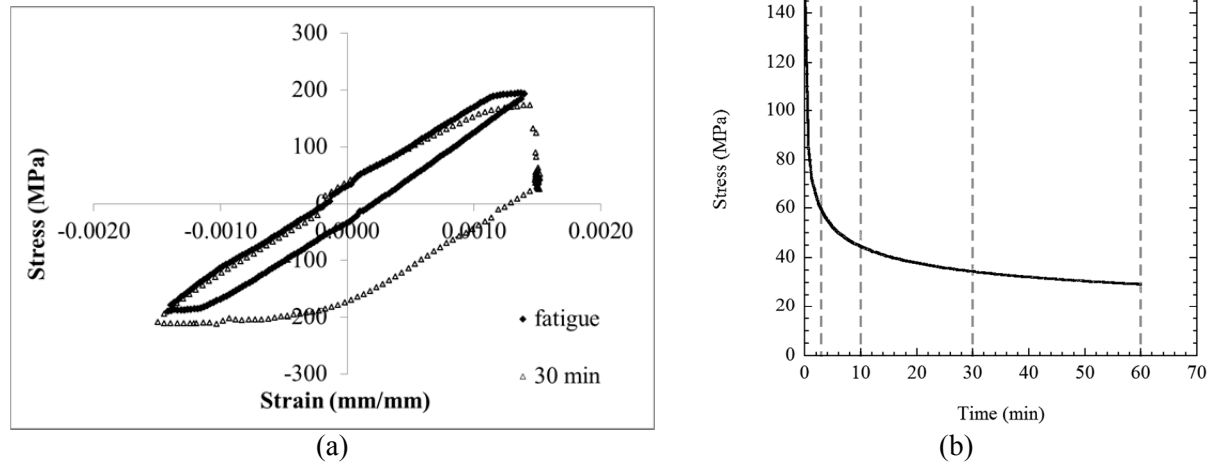


Figure 4. A midlife fatigue and 30-minute hold creep-fatigue hysteresis loops from selected tests at 850°C and 0.3% total strain (a). A midlife stress relaxation fit for the peak tensile strain controlled hold time at 850°C and 0.3% total strain (b).

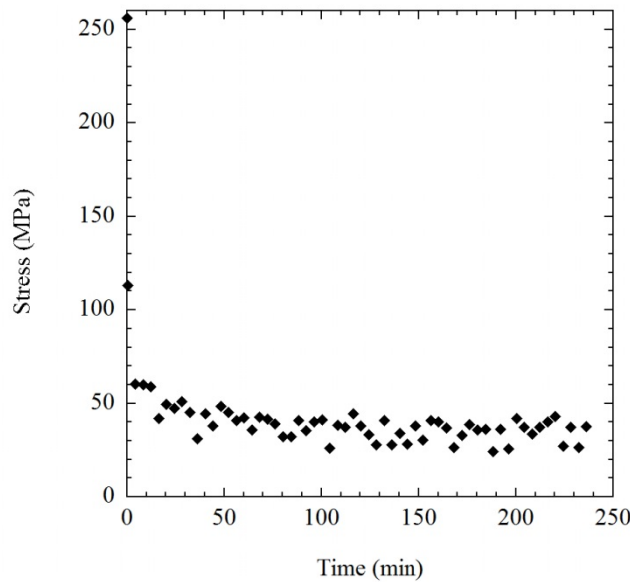
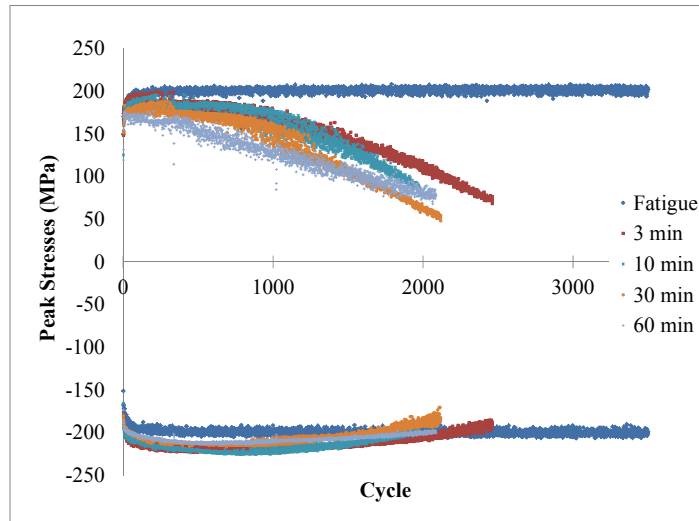
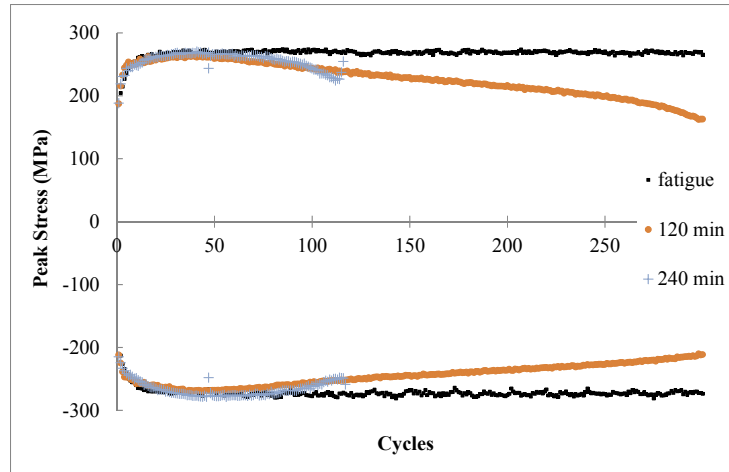


Figure 5. Stress versus hold time during the strain controlled hold for a midlife cycle of a 1.0% total strain creep-fatigue test with a 240-minute hold time.

In fatigue, the peak tensile and compressive stresses reach a steady state value with cycle relatively quickly, as shown in Figure 6. The addition of a tensile hold time during cycling at 0.3% total strain resulted in a decreasing trend in the peak tensile stresses around cycle 500 for the 60-minute hold time condition and closer to cycle 800 or 900 for the 3-minute hold time Figure 6(a). The appearance of a discontinuity in the peak tensile stress versus cycle curve near cycle 250 at the 0.3% strain range is likely caused by the dissipation of dynamic strain aging. Dynamic strain aging can result in slightly higher peak tensile stresses after compressive strain excursions,<sup>9</sup> potentially adding superficially high stress values. Creep-fatigue cycling with hold times less than 30 minutes resulted in a slight initial hardening regime after which the tensile peak stresses decreased dramatically. At the higher strain range of 1.0% total strain, the peak stress versus cycle curves initially exhibit a similar shape as the 0.3% total strain curves, as shown in Figure 6(b).



(a)



(b)

Figure 6. Peak tensile and compressive stresses as a function of cycle for selected continuous-cycle fatigue and creep-fatigue tests at 850°C and 0.3% (a) and 1.0% (b) total strain.

Additionally, as the tensile hold time becomes as long as 60 minutes, a clear hardening regime is no longer observed. One of the two specimens tested at 0.3% total strain and a 60 minute hold time did not exhibit an obvious point of macrocrack initiation, based upon the stress ratio versus cycle plot. In the peak

stresses versus cycle plot, shown as light blue in Figure 6(a), continued degradation of the peak tensile stress is observed to more than 2,000 cycles, however, because of the extensive interior grain boundary damage present, this specimen had clearly “failed” despite the inability to assign an  $N_f$  value. For this condition, it appears that the method of assigning  $N_f$  is not representative.

### 3.2 Deformed Microstructures

Cycling in fatigue resulted in a primary transgranular surface crack. There also was no evidence of interior grain boundary cavitation or cracking in the deformed fatigue specimens. In creep-fatigue at the 1.0% total strain and 3-minute hold condition the mode of surface crack propagation was also transgranular. For the 10-minute hold time at 1.0% total strain, the cracking mode is mixed while longer hold times resulted in the primary crack propagation mode being intergranular. For the 120 minute hold time condition, the specimen exhibited many intergranular, secondary cracks along surface connected, oxidized grain boundaries. The microstructure in the regions surrounding these cracks was depleted of carbides. An oxide layer was present on the crack flanks of the primary and secondary cracks. At the 1.0% strain range the surface cracks, whether primary or secondary, dominate the damage visible optically. Interior grain boundary cracks were present following creep-fatigue deformation at the 1.0% strain range but they were limited. At the longer hold times, 120 and 240 minutes, the interior grain boundary cracks were concentrated near regions surrounding a primary surface crack. The grain boundaries in the areas further from the primary crack had a very limited amount of interior cracking. The primary and secondary cracking modes as well as the presence of interior grain boundary cracks are summarized in Table 2.

Table 2. Cracking modes observed in fatigue and creep-fatigue specimens tested at 850°C selected for metallurgical evaluation.

	Primary Cracking Mode	Secondary Cracking Mode	Interior Grain Boundary Cracking
<b>0.3% total strain</b>			
fatigue	Transgranular	None	No
3 minutes	Mixed	Primarily intergranular	Yes
10 minutes	Primarily Intergranular	Intergranular	Yes
30 minutes	Intergranular	Intergranular	Yes
60 minutes	Intergranular	Intergranular	Yes
<b>1.0% total strain</b>			
fatigue	Transgranular	Transgranular	No
3 minutes	Transgranular	Transgranular	Limited
10 minutes	Mixed	Transgranular	Limited
30 minutes	Intergranular	Both	Yes
120 minutes	Intergranular	Intergranular	Concentrated regions, limited elsewhere
240 minutes	Intergranular	Intergranular	Concentrated regions, limited elsewhere

Creep-fatigue cycling at 0.3% total strain also resulted in the primary crack propagation mode evolving from mixed mode to intergranular with increasing hold times, as shown by the example of the primary cracks in a pure fatigue and 30-minute hold time specimen in Figure 7.

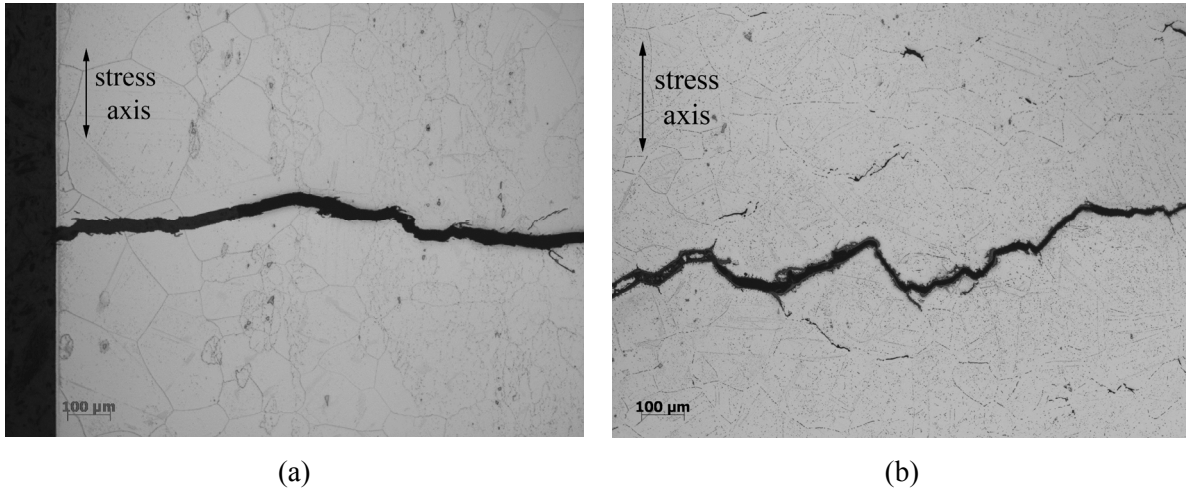


Figure 7. A transgranular surface crack in a 0.3% total strain fatigue specimen cycled at 850°C (a). An intergranular surface crack in a 0.3% total strain, 30-minute hold creep-fatigue specimen cycled at 850°C (b). The specimen surface is not shown in (b) but is to the left of the image.

The primary crack path in the 30-minute hold time specimen was predominantly intergranular. Additionally, many secondary surface cracks with primarily intergranular character were evident following creep-fatigue deformation. The deformed creep-fatigue specimens contained grain boundary cracks in the specimen interiors, as illustrated for the 0.3% and 3-minute hold time condition in Figure 8. The interior grain boundary cracks were present throughout the specimen interior. It was previously reported<sup>10</sup> that the amount of interior grain boundary cracking increased with increasing hold time and no interior grain boundary cracking was present at the 3-minute hold time. Multiple additional 3-min hold time creep-fatigue specimens, however, were metallographically analyzed and extensive interior grain boundary cracking was observed in these specimens. This discrepancy is currently being investigated in more detail, but the specimen investigated previously<sup>10</sup> did not have an identifiable surface crack and is believed to be an anomaly.

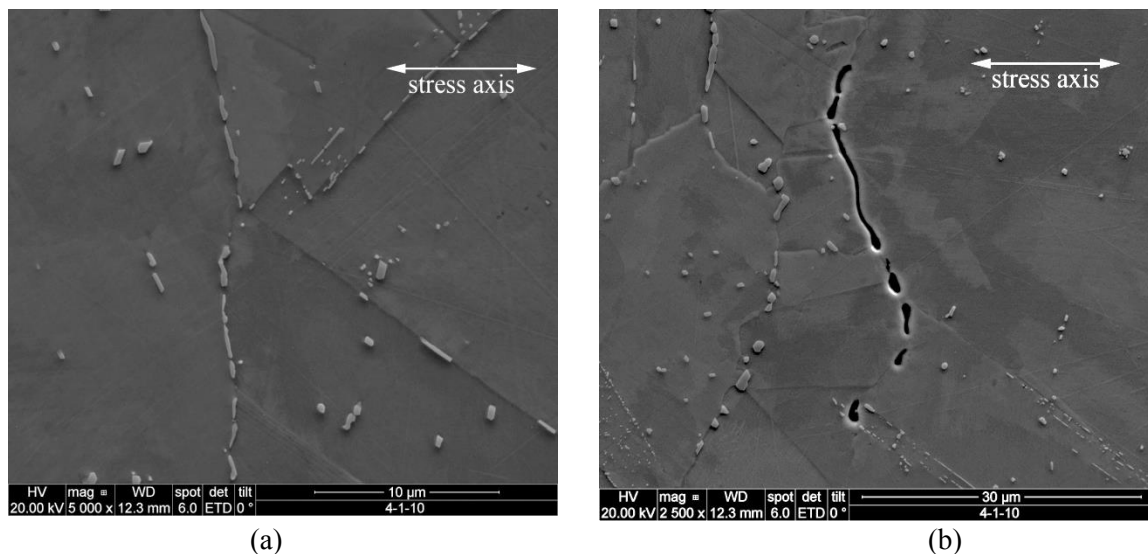


Figure 8. Acicular carbides on an internal grain boundary (a) and grain boundary cavitation/cracking (b) in a creep-fatigue specimen tested at 0.3% total strain and a 3-minute hold time at 850°C.

The development of grain boundary cracking throughout the specimen interior at the 0.3% strain range and 3-minute tensile-hold creep-fatigue condition was studied through testing of multiple specimens with specific interruptions. A consistent cross-sectional area, encompassing the approximate gage section lengthwise, was analyzed to quantify the interior grain boundary cracks. Interruptions represented a point near the maximum of the peak stress versus cycle curve (1,000 cycles) and points along the curve in the cyclic softening regime, as illustrated in Figure 9. Almost all of the grain boundary length was intact after 1,000 cycles. The total cracked grain boundary length increased as the cycling progressed further. Quantified as a fraction of the total amount of cracked grain boundary length at test completion; approximately 5% of the cracked boundary length was present by cycle 1,500 and 30% by Cycle 2000. The remaining cracked boundaries occurred after Cycle 2,000, consistent with the rapid drop in the peak tensile stress.

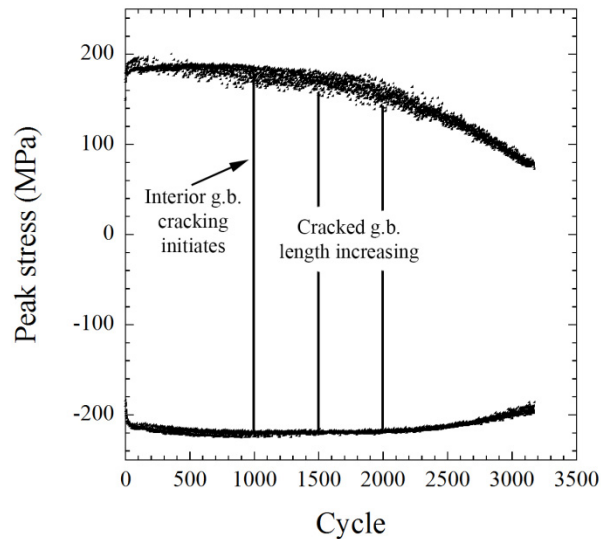


Figure 9. A plot of the peak stress versus cycle data with the progression of the interior grain boundary cracking superimposed from a creep-fatigue specimen tested at 0.3% total strain and a 3-minute hold time at 850°C.

### 3.3 Dislocation Substructures

A significant amount of grain-to-grain variation is observed in the local dislocation substructure of the deformed material and generalized descriptions regarding these substructures are made here with that understanding. Grain sizes and shapes can vary greatly throughout the bulk specimen depending on the inherent irregularity of carbide distributions. Numerous observations have been compiled to capture and classify the most representative microstructures at the length scales of subgrains. Subgrains are distinguished from cells in that the boundaries consist of distinctly ordered arrangements of dislocations as opposed to tangled dislocations in a cell wall.

The creep-fatigue substructure at failure was investigated for the 0.3% total strain range and consists of subgrains with well-organized boundaries of arrays or networks of dislocations, as shown in Figure 10. The size of the subgrains varies, although they are generally on the order of 5 to 10  $\mu\text{m}$ . The subgrain interiors contain many uniformly distributed mobile dislocations. The mobile dislocation density throughout the subgrain interiors is much greater than in the creep-fatigue specimens deformed at 950°C.<sup>3</sup> Fatigue deformation also resulted in the material having a dislocation structure consisting of subgrains with mobile dislocations in the interiors, despite the absence of a hold time, as shown in Figure 11.



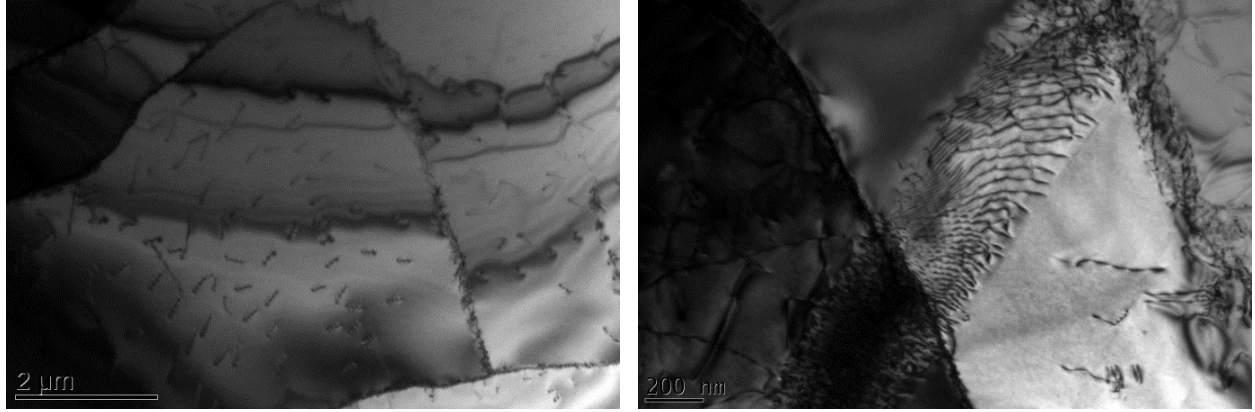


Figure 10. TEM images from the deformed gage section of creep-fatigue specimens tested at 850°C and the 0.3% total strain range and a 30-minute (a) and a 10-minute (b) peak tensile hold.

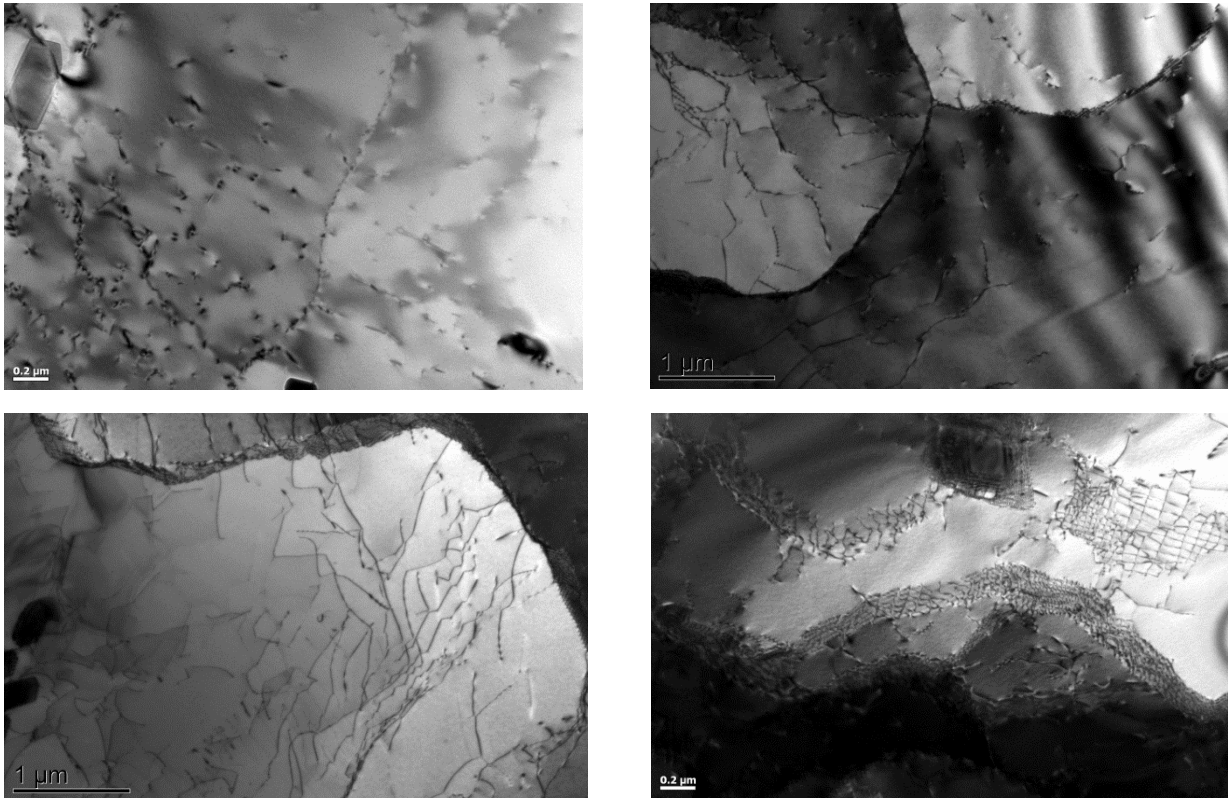


Figure 11. TEM images illustrating the subgrain structure in the gage section of continuous-cycle fatigue specimens tested at 850°C and the 0.3% total strain range.

TEM analysis of the dislocation structure at the specific interruptions at the 0.3% strain range and 3-minute tensile-hold condition revealed that by 1,000 cycles, a subgrain structure has formed and the subgrain diameters are on the order of 5 to 10  $\mu\text{m}$ , as shown in Figure 12. Based on a quantification of multiple regions using a line intercept method and assuming a foil thickness of 75  $\mu\text{m}$ , the subgrain interiors contained a mobile dislocation density of approximately  $4 \times 10^{13}/\text{m}^2$ . The dislocation substructure was similar at 1,500 cycles and again at 2,000 cycles, also shown in Figure 12. The mobile dislocation density after 2,000 cycles averaged  $6 \times 10^{13}/\text{m}^2$  and the subgrain diameters were similar in size to those observed at 1,000 cycles. The dislocation density at the end of life has not yet been



quantified. In summary, the dislocation substructure consisting of subgrains, dislocation pileups, and mobile dislocations is formed by the point at which a plateau in the peak stress is reached and persists through the remainder of the cycle life at the investigated creep-fatigue condition.

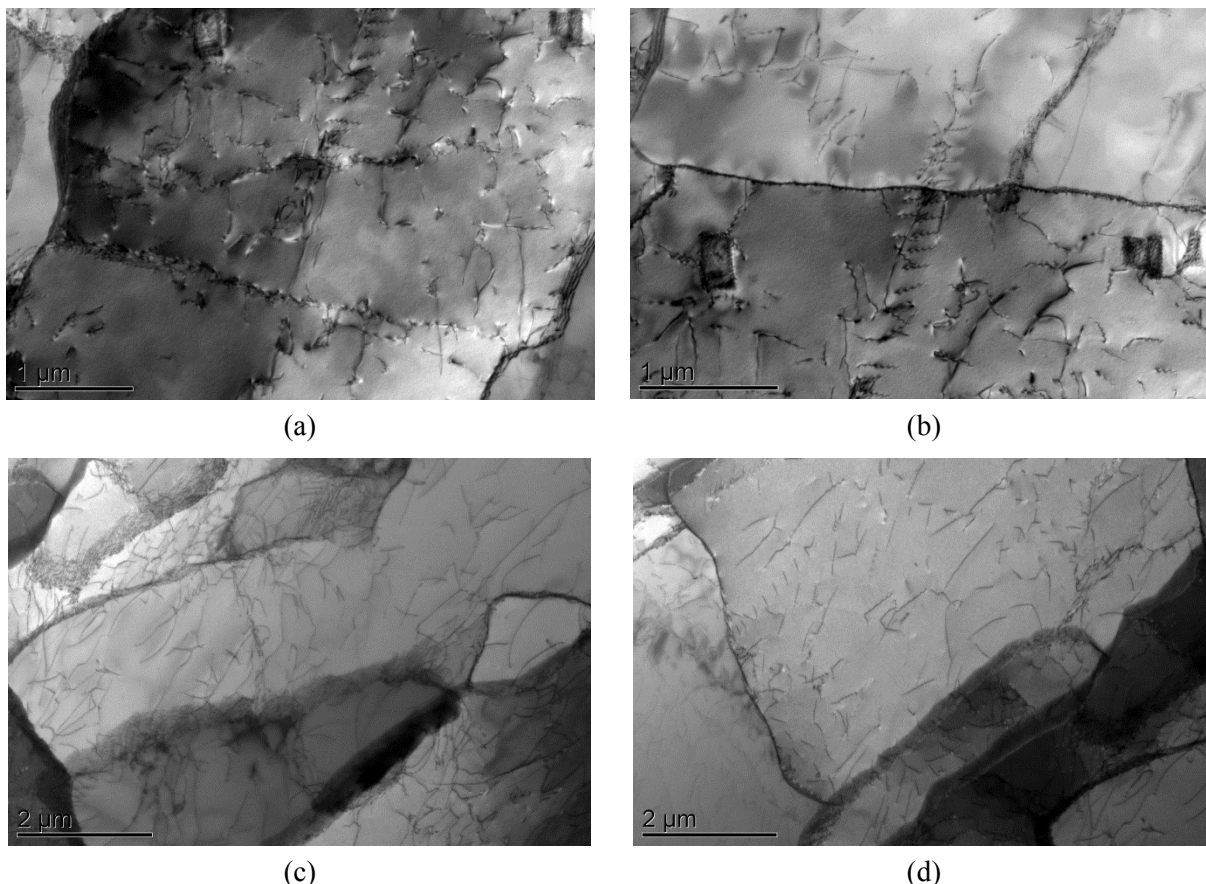


Figure 12. TEM images from the gage section of creep-fatigue specimens tested at 850°C and the 0.3% total strain range and a 3-minute peak tensile hold at 1,000 cycles (a and b) and 2,000 cycles (c and d) .

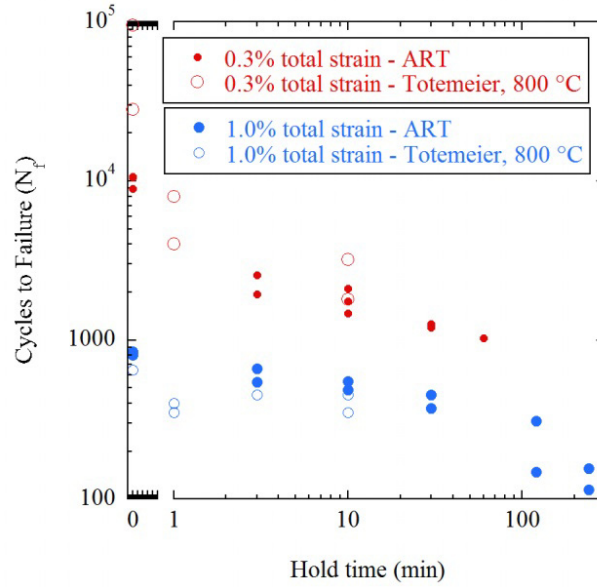
## 4. DISCUSSION

### 4.1 Creep-Fatigue Saturation

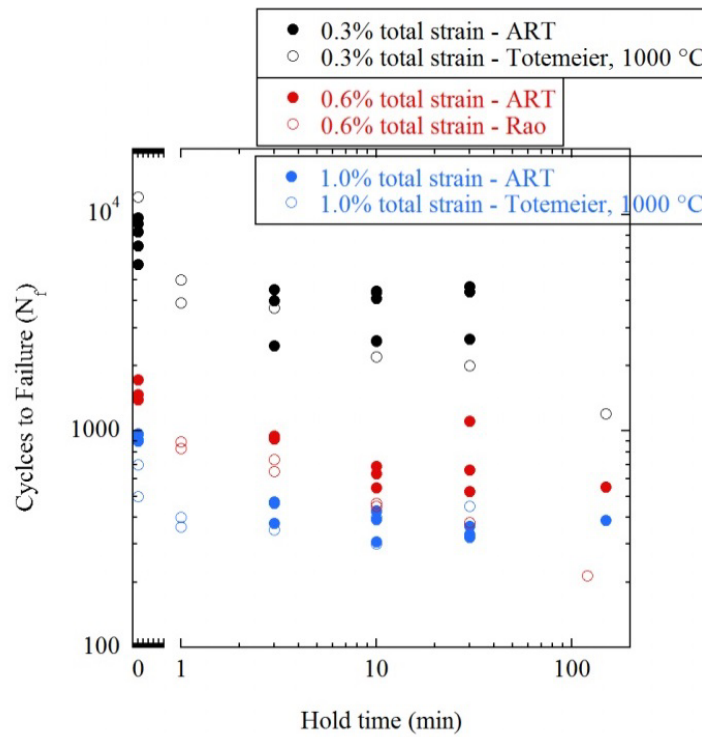
Determination of whether the number of cycles to failure saturates with increasing hold times is a consideration for implementation of Alloy 617 into Subsection NH of the American Society of Mechanical Engineers (ASME) Code. From the data set of Carroll et al., saturation occurs within relatively short hold times at 950°C at the investigated conditions.<sup>2,3</sup> This observation of saturation is not consistent with the work of Rao et al. on Alloy 617 at 950°C in simulated reactor helium,<sup>4</sup> as mentioned in the Introduction and is shown in Figure 13(b). The number of cycles to failure data from Totemeier generated at 1000°C is consistent with the 950 °C data of Carroll et al., yet evidence of saturation in the number of cycles to failure is not present at 0.3% total strain. If the three data sets (at 950 and 1000°C) are taken as a whole, the presence, or lack of, saturation is not clear due to the limited amount of data and replicates at the longest hold time conditions.

At 850°C, the number of cycles to failure continues to decrease between the 30- and 60-minute hold time conditions at the 0.3% total strain range. Similarly, a substantial decrease in the number of cycles to failure is also observed at the 1.0% strain range between the 120- and 240-minute hold time condition.

Totemeier and Tian<sup>11</sup> investigated the creep-fatigue behavior of Alloy 617 at 800°C at the 0.3% and 1.0% strain range for hold times up to 10 minutes and the data are plotted along those of the current work in Figure 13(a). The data from the work of Totemeier and Tian<sup>11</sup> is consistent in magnitude with the cycles to failure for 850°C presented herein. The Totemeier and Tian data<sup>11</sup> does appear to saturate at the 1.0% strain range for the moderate duration hold times tested. At 0.3% total strain, saturation in the number of cycles to failure was not observed by Totemeier and Tian,<sup>11</sup> consistent with the results reported herein at 850°C. In general, saturation of the creep-fatigue number of cycles to failure as a function of hold time should not be expected at 800 or 850°C.



(a)



(b)

Figure 13. Alloy 617 fatigue and creep-fatigue data from the current work (ART), Rao et al.,<sup>4</sup> and Totemeier and Tian<sup>11</sup> (the values of which have been estimated from published papers). The data from Rao<sup>4</sup> was generated in a simulated helium environment and that of Totemeier et al.<sup>11</sup> at 800 and 1000°C. The 150 minute hold time ART data point at 950 °C and the 0.6% strain range was a runout, as indicated by the arrow.

At 850°C, stress relaxation during the strain controlled tensile hold exhibits higher initial stresses and higher relaxed stresses than at 950°C. Additionally at 850°C, the stresses continually decrease with time throughout the hold at the 0.3% strain range for hold times of up to 60 minutes (Figure 4(b)), whereas at the 1.0% strain range, the stress relaxation curve does appear to plateau prior to completion of the longest hold time condition: 240 minutes (Figure 5). Despite the rapid stress relaxation and a plateau in the stress relaxation curve at the higher strain range at 850 °C, there is no evidence from the experimental data that saturation of the number of cycles to failure with increasing hold durations is achieved. Based upon the current trend, further increases in hold time duration beyond 240 minutes (at 1.0% total strain) are likely to continue to reduce the number of cycles to failure. The crack path is intergranular for all but the shortest hold times, indicating an influence of creep and/or the environment. Particularly evident at the 1.0% strain range and the longer hold times, the interior grain boundary cracking does not appear to have a dominant role. Therefore, it is suggested that the longer environmental exposures during the strain controlled hold duration causes additional environmental degradation and thus accelerated creep-fatigue failures.

## 4.2 Cyclic Softening

Cyclic softening arises from the evolution of any of a number of microstructural features, including microcracking, rearrangement or coarsening of the dislocation substructure, a decrease in dislocation-dislocation interactions, and/or precipitate shearing. At 950°C, the decreasing peak tensile stresses were attributed to a combination of microcracking and the evolution of cell walls from tangled dislocations into ordered hexagonal dislocation networks through the rearrangement of dislocations by climb processes, as well as the incorporation of gliding dislocations from the cell interiors into the ordered boundaries.

The macroscopic peak stress versus cyclic behavior at 850°C differs from that at 950°C. At 850°C, hardening is initially exhibited by an increase in the peak stresses, followed by gradually decreasing peak stresses. At the 0.3% total strain and 3-minute hold condition, the decreasing peak stresses directly correlate with the formation of interior grain boundary cracks. The interior grain boundary cracking results in a loss of load bearing cross-sectional area, likely accounting for the decline in peak stresses. Subgrains with well-organized networks of dislocations comprising the boundaries and interiors containing a significant mobile dislocation density form prior to the initial decline in stresses. They persist in a manner, size, and mobile dislocation density, which does not suggest contribution to the decreasing peak stresses. The presence of mobile dislocations in the subgrain interiors allows for continued dislocation-dislocation interactions that likely initially contribute to the hardening process but are not capable of counteracting the strength loss due to the continual reduction in load bearing area as the test proceeds. The presence of mobile dislocations in the subgrain interiors that interact with one another is not observed following creep-fatigue deformation at 950°C.<sup>3</sup>

## 4.3 Damage Diagram

In the ASME Boiler and Pressure Vessel Code, Section III, Subsection NH,<sup>12</sup> creep-fatigue life is evaluated by a linear summation of fractions of cyclic damage and creep damage. The creep-fatigue criterion is given by:

$$\underbrace{\sum_j \left( \frac{n}{N_d} \right)_j}_{\text{Cyclic Damage}} + \underbrace{\sum_k \left( \frac{\Delta t}{T_d} \right)_k}_{\text{Creep Damage}} \leq D$$

where  $n$  and  $N_d$  are the number of cycles of type  $j$  and the allowable number of cycles of the same cycle type, respectively; and  $\Delta t$  and  $T_d$  are the actual time at stress level  $k$  and the allowable time at that stress level, respectively;  $D$  is the allowable combined damage fraction. The cyclic- and creep-damage terms on

the left-hand side of the above equation are evaluated in an uncoupled manner, and the interaction of creep and fatigue is accounted for empirically by the  $D$  term on the right side of the equation.

Details of the analysis method have been outlined by T. L. Sham.<sup>13</sup> In short, the fatigue (cyclic) damage fraction,  $D^f$ , for a creep-fatigue test is defined in terms of the ratio of the cycles to failure,  $n$ , under creep-fatigue conditions to the number of cycles to failure,  $N_d$ , under continuous cycling conditions for the same product form and heat, and at the same total strain range and temperature, as the creep-fatigue test. Data for more than one continuous cycling test was available at the same total strain range and temperature, thus their average was used for the value of  $N_d$ , as best estimate values will be used for establishing the envelope of the interaction curve in the D-diagram.

The creep damage for the  $k^{th}$  creep-fatigue cycle,  $D_k^c$ , is determined by evaluating the integral:

$$D_k^c = \int_{hold\ time} \left( \frac{1}{T_d} \right)_k dt$$

over the hold time of the cycle. Summing the total creep damage accumulated during a creep-fatigue test would require information on the stress history during the hold time for all the cycles. An approximation commonly made in calculating the total creep damage is to evaluate the creep damage for a midlife cycle, and multiply this value by the total number of cycles to failure. The stress relaxation data during a strain hold period was fit to a power-law trend curve using the following functional form:

$$\sigma = b_0 (t + t_0)^{b_1}$$

where  $b_0$ ,  $b_1$ , and  $t_0$  are treated as fitting parameters,  $\sigma$  is in units of MPa, and  $t$  and  $t_0$  are in units of seconds. The information is then substituted into the creep damage equation for the  $k^{th}$  cycle. To perform the integration, the correlation between the rupture time, temperature, and applied stress for the heat of Alloy 617 under consideration is required. Since this correlation is not yet available, that of Eno et al. determined by a best-estimate correlation from an Alloy 617 database, using the Mendelson-Roberts-Manson time-temperature-stress parameterization<sup>14</sup> was utilized instead. The same database was used by Corum and Blass<sup>15</sup> in the development of the Draft Alloy 617 Code Case and by Eno et al.<sup>14</sup> in developing the time-dependent stress limits for a space reactor application.

Preliminary  $D$  values for each of the creep-fatigue data points for Alloy 617 at 850 and 950°C<sup>10</sup> were calculated and placed on the D-diagram, as shown in Figure 14. For reference, the D diagram plot also includes the creep-fatigue envelope recommended in the Draft Alloy 617 Code Case, which has an intersection at coordinates (0.1, 0.1).<sup>14</sup> The preliminary calculations of the  $D$  values fall on both sides of the recommended creep-fatigue envelope, and tend to group according to test conditions. It should, however, be noted that all of the qualified and trend data points have been included. Further analysis will need to separate the trend data points and confirm that they are within the scatter band of the qualified data points. For the long hold creep-fatigue conditions, most representative of operating conditions, at 850°C the points are near the (0.1, 0.1) intersection point or below, as is illustrated in Figure 15. The 0.3% total strain, 3- and 10-minute hold data have the highest creep damage values; all but one point have a  $D_c$  value of greater than 0.2 and relatively low values of fatigue damage,  $D_f$  (Figure 16). To achieve even higher  $D_c$  values for the D-diagram it is recommended that creep-fatigue testing be conducted at a lower temperature such as 800°C and that the data of Totemeier and Tian<sup>11</sup> be considered. The lower temperature cycling exhibits higher stresses during the strain-controlled hold time, which results in higher  $D_c$  values.

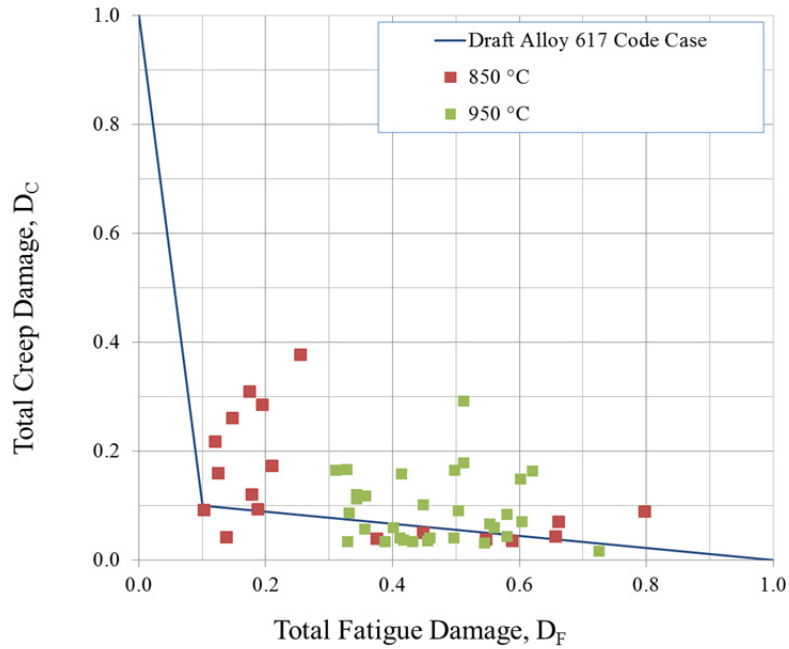


Figure 14. Preliminary values for the creep-fatigue damage diagram data points calculated for the 850 and 950°C using the midlife cycle to assess the creep damage term and the creep-fatigue envelope (blue line) recommended during the Draft Alloy 617 Code Case.<sup>14</sup>

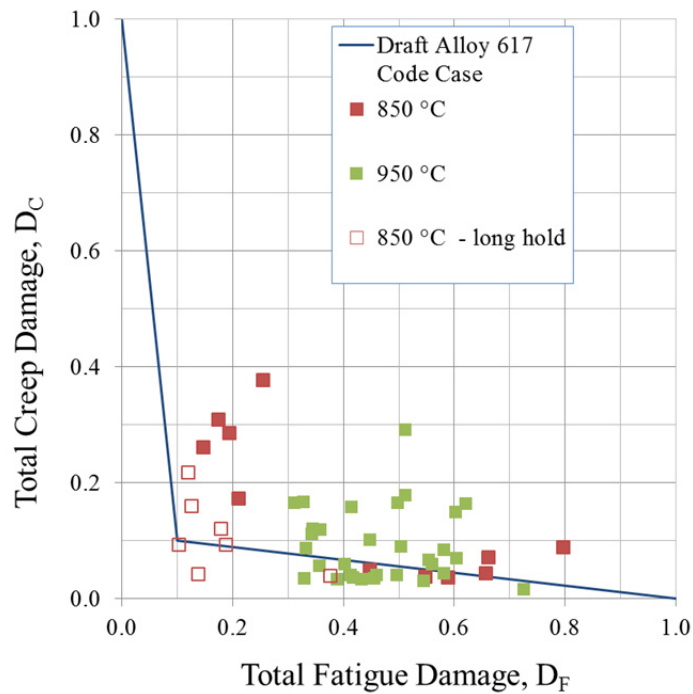


Figure 15. Preliminary values for the creep-fatigue damage diagram data points calculated for 850 and 950°C and the creep-fatigue envelope (blue line) recommended during the Draft Alloy 617 Code Case.<sup>14</sup> The 850°C long hold (0.3% strain range and a 30-minute hold time or longer and 1.0% strain range and a 120-minute hold time or longer) data points are a separate data series labeled 850°C – long hold.

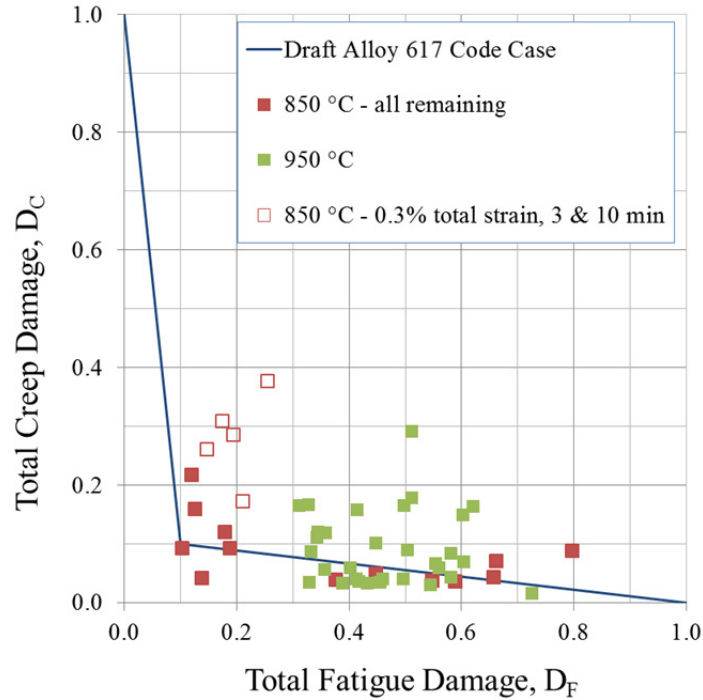


Figure 16. Preliminary values for the creep-fatigue damage diagram data points calculated for the 850 and 950°C and the creep-fatigue envelope (blue line) recommended during the Draft Alloy 617 Code Case.<sup>14</sup> The 0.3% strain range and 3- and 10-minute hold times exhibit the highest  $D_C$  values.

## 5. CONCLUSIONS

The creep-fatigue behavior of Alloy 617 at 850°C varies dramatically from the behavior at 950°C. In terms of the total number of cycles to failure, a strain controlled tensile hold of up to 60 minutes at the 0.3% strain range and 240 minutes at the 1.0% strain range does not result in saturation. Longer hold times continue to degrade the creep-fatigue resistance. The creep-fatigue deformation mode is dependent on the strain range/hold time conditions; however, at relatively short hold times the crack propagation mode became intergranular. Based upon analysis of interrupted creep fatigue specimens tested at a low strain range and 3-minute hold time, the interior grain boundary cracking is the major contributor to tensile-side cyclic softening. Additionally, preliminary values for the creep-fatigue damage diagram have been calculated and fall on both sides of the envelope when a (0.1, 0.1) intersection is considered.

## 6. REFERENCES

1. Wright, J. K., Wright, R. N., and Sham, S., 2010, *Next Generation Nuclear Plant Steam Generator and Intermediate Heat Exchanger Materials Research and Development Plan*, PLN-2804, Idaho National Laboratory, September 2010.
2. Carroll, L. J., Cabet, C., Carroll, M. C., and Wright, R. N., 2013, "The development of microstructural damage during high temperature creep-fatigue of a nickel alloy," *International Journal of Fatigue*, Vol. 47, pp. 115-125.
3. Carroll, M. C., and Carroll, L. J., 2013, "Developing Dislocation Subgrain Structures and Cyclic Softening During High-Temperature Creep-Fatigue of a Nickel Alloy," *Metallurgical and Materials Transactions*, Vol. 44, No. 8, pp. 3592-3607.
4. Rao, K. B. S., Meurer, H. P., and Schuster, H., 1988, "Creep-Fatigue Interaction of Inconel 617 at 950°C in Simulated Nuclear Reactor Helium," *Materials Science and Engineering*, Vol. 104, pp. 37-51.
5. Totemeier, T. C., and Tian, H. B., 2007, "Creep-fatigue-environment interactions in INCONEL 617," *Materials Science and Engineering*, Vol. 468, pp. 81-87.
6. Carroll, M. C., and Carroll, L. J., 2012, "Fatigue and Creep-fatigue Deformation of an Ultra-fine Precipitate Strengthened Advanced Austenitic Alloy," *Materials Science and Engineering*, Vol. 556, pp. 864-877.
7. Kesternich, W., 1985, "Dislocation-controlled precipitation of TiC particles and their resistance to coarsening," *Philosophical Magazine*, Vol. 52, pp. 533-548.
8. Challenger, K. D. and Moteff, J., 1972, "Characterization of the deformation substructure of AISI 316 stainless steel after high strain fatigue at elevated temperatures," *Metallurgical and Materials Transactions*, Vol. 3, pp. 1675-1678.
9. Creep-Fatigue Testing, INL/PLN-3346 Rev. 8.
10. Carroll, L. and Carroll, M., 2013, *Creep-Fatigue Behavior of Alloy 617 at 850 and 950°C*, INL/EXT-13-28886, Rev.3, Idaho National Laboratory, May 2015.
11. Totemeier, T. C., 2008, "High-temperature creep-fatigue of alloy 617 base metal and weldments, Proceed. ASME Press," *Vessels Piping Conference*, Vol. 9, pp. 255-260.
12. ASME, 2013, *ASME Boiler and Pressure Vessel Code, Section III, Division 1, Subsection NH, Class 1 Components in Elevated Temperature Service*, ASME, New York.
13. Wright, J. K., and Sham, S., 2010 "Creep-Fatigue Interaction Diagram for Alloy 617 in Air at 950°C," ECAR-1199, Idaho National Laboratory, September 2010.
14. Eno, D. R., Young, G. A., and Sham, T. L., 2008, "A Unified View of Engineering Creep Parameters," *ASME 2008 Pressure Vessels and Piping Conference*, Paper No. PVP2008-61129, pp. 777-792.
15. Corum, J. M., and Blass, J. J., 1991, "Fatigue, Fracture, and Risk-1991," *ASME 2008 Pressure Vessels and Piping Conference*, Vol. 215, pp. 147-153.